Influence of AM Generated Burner Surface Roughness on NO$_x$ Emissions and Operability of Hydrogen-Rich Fuels

Ianos Psomoglou, Burak Goktepe, Andrew Crayford, Phil Bowen, Steve Morris & Nick Jones

Published online: 16 Aug 2024.

Submit your article to this journal ⬈

Article views: 32

View related articles ⬈

View Crossmark data ⬈

Taylor & Francis
Taylor & Francis Group

Influence of AM Generated Burner Surface Roughness on NO$_x$ Emissions and Operability of Hydrogen-Rich Fuels

Ianos Psomoglou[a], Burak Goktepe[a], Andrew Crayford[a], Phil Bowen[a], Steve Morris[a], and Nick Jones[b]

[a]School of Engineering, Cardiff University, Cardiff, UK; [b]R&D department, Renishaw Plc, Gloucester, UK

ABSTRACT

The additive manufacturing (AM) technique enables the fabrication of advanced burner components to enhance the hydrogen capability of the existing gas turbines (GTs) and reduce the carbon footprints of the power generation sector. This technique produces rough surfaces that may require post-processing to maintain the desired functionality of a burner, particularly for hydrogen fuel with unique thermo-physical properties. This study, therefore, compared the stability of three swirlers of variable surface roughness manufactured using AM and traditional machining methods, with one of the AM swirler post-processed by grit-blasting. The comparison included a conventional benchmark (100% CH$_4$), low carbon (23%$_{vol}$CH$_4$/77%$_{vol}$H$_2$) and zero carbon (100% H$_2$) fuels across a range of equivalence ratios. Additionally, the study quantified the flame topology and emissions performance of the fuel blends for each swirler using high-speed OH* chemiluminescence and exhaust gas emissions measurements, respectively. The experimental investigation concluded that the AM-generated surface roughness within the considered range does not detrimentally impact NO$_X$ emissions and the stability of the fuel mix. However, the flame location was observed to be influenced by surface roughness and shifted more toward the vertical centerline of the burner with increased roughness. From the practical perspective, the results showed that post-manufacturing surface finishing offers negligible performance advantages, indicating potential cost reductions. It is recommended that further studies should investigate the influence of increased surface roughness on burner performance, as well as numerical modeling techniques which could provide an insight into when AM surfaces are likely to be more influential.

Introduction

Additive Manufacturing (AM), also known as Additive Layer Manufacturing (ALM) or 3D printing, has been introduced as a pioneering manufacturing technique over the past 10 years. It has the potential to revolutionize industries with the power generation and biomedical sectors being two notable examples. This innovative manufacturing technique enables the fabrication of enhanced structures of complex geometry, previously not possible through subtractive methods. Additionally, it offers several advantages, including multiple-component integration, rapid prototyping, freedom of design,

CONTACT Ianos Psomoglou ✉ psomogloui@cardiff.ac.uk; ianps96@gmail.com ✉ School of Engineering, Cardiff University, 12 Elikonos street, Cardiff, Wales CF10 3AT, UK

minimization of material waste, and lead time, as well as multifunction components of novel internal structures, making AM superior to conventional manufacturing techniques (Ngo et al. 2018). In the biomedical sector, these advantages promote the fabrication of customized end-products, through more efficient and simplified supply chain systems of minimal waste, greatly improving quality of life and sustainability index (Velu et al. 2020). In the context of the gas turbine (GT) industry, AM also has the potential to address challenges linked to material properties and combustion inefficiency, associated with flashback, unburnt fuel, elevated emissions, and combustion instabilities (ETN Global 2020). Therefore, AM could greatly contribute to sustainability by promoting the utilization of low and zero-carbon fuels (e.g., H_2, NH_3, $NH_3/H_2/CH_4$ blends) to enable a smoother transition from fossil-fuel-based heat and power toward a more renewable supply, with lower harmful greenhouse gas emissions and other gaseous pollutants, such as NO_x emissions (ETN Global 2020, National Academies of Sciences, Engineering, and Medicine 2020).

Hydrogen has been gaining attraction as an alternative to fossil fuel use in automotive and GT systems. It can be produced from various renewable or nonrenewable feedstocks and chemical processes and serve as an energy storage medium for carbon-free power generation. Hydrogen supports the electrification of transportation through Fuel Cell Electric Vehicles (FCEVs) and power-to-gas economy through "Green" hydrogen. It can be used to generate electricity or it can be blended with other carbon sources to produce fuels such as syngas or methane (Goldmeer 2019; Jayakumar et al. 2022). For the given potential of AM applications to hydrogen utilization, GT market-leading Original Equipment Manufacturers (OEMs) have already invested in utilizing metallic AM technology for the development and seamless manufacturing of novel GT components. This secures the role of GTs in energy transition and renewable energy installations (ETN Global 2020National Academies of Sciences, Engineering, and Medicine 2020; Runyon et al. 2021). Numerous examples of AM development have accommodated hydrogen utilization both in academia (Fan et al. 2021; An et al. 2021) and in industry (Larfeldt et al. 2017; Patel 2018; Prandi 2019; Walton 2021). Projects such as those by the US Department of Energy and ongoing European projects, aim to demonstrate the performance of AM combustion systems and components in high $H_2/syngas$ (York et al. 2015), and zero-carbon H_2/NH_3 GT (UK Research and Innovation 2020). Other examples include AM-based burner tip temperature improvements for high H_2 operation and innovative AM nozzle designs and fuel injector patents, regarded for hydrogen combustion applications (Runyon et al. 2021).

Furthermore, a unique advantage that AM offers is the fabrication of specific, predefined surface roughness, depending on the selected build parameters employed during manufacture. As rough surfaces can influence boundary layer fluid flow and hence the operation and the efficiency of the GT systems significantly, the investigation of surface texture, as a function of building parameters and resultant surface roughness, has become a focused area of research (Bons et al. 2008; Mumtaz and Hopkinson 2010). The alteration of the roughness texture of GT blades and stator due to prolonged operation, fuel deposits, corrosion, erosion, and thermal barrier coating constitute some of the most common issues associated with surface roughness and GTs. A review of these and related issues may be found in Bons (Bons 2010). Consequently, due to the importance of surface roughness and its synergy with GT

operation, the influence of the former on the latter has recently gained scientific interest (Al-Fahham, Bigot, and Valera Medina 2016; Crayford et al. 2019; Hatem et al. 2017; Runyon et al. 2019).

The investigation of the effects of surface roughness on fluid flows started over a century ago (Darcy 1857; Fanning 1886). Since then, experimental and numerical studies of the effects of surface roughness on heat transfer, as well as on isothermal and reacting flows, have been conducted, as reviewed thoroughly by Kadivar et al. (Kadivar, Tormey, and McGranaghan 2021). In summary, when the roughness height is above an "admissible" value, it interacts with the boundary layer modifying its characteristics. Thus, the transition of the boundary layer from laminar to turbulent, as well as the separation susceptibility of the flow, are influenced, ultimately affecting the overall *form drag* (Schlichting and Gersten 2014). Furthermore, surface roughness often increases skin-friction (Moody 1944; Nikuradse 1950), consequently increasing the overall pressure drop, which is a function of both *skin-friction*-related drag and *form*-related drag (Schlichting and Gersten 2014). However, it has been proposed that surface roughness potentially has a positive impact on GT performance. Several studies have shown that "manufacturable roughness" can potentially improve the performance of GT components by enhancing its heat transfer and aerodynamic characteristics (Dean and Bhushan 2010; Domel et al. 2018; Li, Guo, and Huang 2020; Liu et al. 2020). Analogous to the dimpled surface of golf-balls, biomimetic textures, such as shark-skin, have been found to reduce aerodynamic drag whilst enhancing heat transfer due to promoted turbulent mixing near the wall (Al-Fahham et al. 2017; Dean and Bhushan 2010; Hatem et al. 2017). In the context of combustion instabilities, the introduction of such a geometry in a generic swirl burner resulted in reduced boundary layer flashback propensity without modifying the bulk geometric characteristics of the burner (Al-Fahham et al. 2017; Hatem et al. 2017).

As for conventionally manufactured GT parts, AM-manufactured ones that fail to meet the desired functional criteria upon printing, often subject to post-processing, such as grit-blasting, to reduce the surface roughness height and ultimately improve surface quality (Lu et al. 2023; Sinha et al. 2022). However, since this activity increases total lead-time and cost of production, both profitability and the necessity of such action is an active area of interest (Liu et al. 2023). Of particular interest to the present study is the experimental campaign carried out by Runyon et al. (2019), in which two additively manufactured swirlers (of which, one was post-processed via grit-blasting, and one was left raw) of different average surface roughness height were compared against a conventionally manufactured "smooth" swirler. The two AM swirlers, which were tested under 100% CH_4 combustion and atmospheric pressure conditions, resulted in improved combustion performance, with respect to NO_x emissions, whilst also being found to affect flame stabilization location. However, although there is scattered evidence of the potential of "manufacturable roughness" derived from AM, the investigation of the influence of surface roughness on specific combustion phenomena is still overlooked.

Motivated by the aforementioned challenges, the current status of synergy between AM and GT, and a previous experimental campaign (Runyon et al. 2019), the present study aims to gain an empirical understanding of the influence of surface roughness and its post-processing requirements on emissions characteristics and combustion performance of a generic AM swirl burner fueled on blends ranging from conventional methane to pure hydrogen across a range of equivalence ratios.

Experimental methods

Methodology

The experimental program aimed to investigate the effect of surface roughness on lean-premixed swirling flames under atmospheric pressure and elevated inlet temperature conditions. A first database of well-controlled experiments was generated at Cardiff University's Gas Turbine Research Centre (GTRC).

The study investigated three different fuel blends, including conventional (100% CH_4), low carbon (77%$_{vol}H_2$/23%$_{vol}CH_4$) and zero carbon (100% H_2) fuels. Hydrogen-rich fuel blends were selected to analyze the interaction of surface roughness given premixed hydrogen flames are prone to intrinsic thermo-diffusive instabilities (Berger, Attili, and Pitsch 2022), impacting flame shape, heat release, and flame speed. In this study, the CH_4/H_2 ratio in the low carbon fuel blend was determined by considering equal contribution of each fuel to the total thermal power.

To avoid geometric effects on emissions and combustion characteristics of the fuel blends, nominally identical three-dimensional generic swirl burners of different surface roughness were manufactured (Figure 1). Two AM swirlers were deployed, one "grit-blasted" (AM-G) and one "raw" (AM-R), with the average surface roughness height roughly 5 μm and 9 μm, respectively, together with a traditionally manufactured "smooth" swirler (Machined), with an analogous value of 1 μm. Further details on the surface roughness measuring set-up and geometry of the swirlers are found elsewhere (Runyon et al. 2019).

The experimental investigation of the conventional methane flame was used as a benchmark case of the test matrix for the comparative appraisal of low-carbon/hydrogen-rich fuels. In all cases, the thermal power output was kept constant at 25 kW. Thus, only airflow was adjusted to produce necessary changes in the equivalence ratio. Additionally, the airflow determines the bulk flow velocity of the mixture and provides a broad range of Reynolds numbers to examine the influence of surface roughness on flow characteristics. Surface roughness effects were examined through a combined analysis of data involving the operational flame stability map, exhaust emissions, and temperatures. The flame stability map (Lean Blow Off (LBO) and FlashBack (FB) limits) were established over a range of equivalence ratios at inlet temperatures of 150 ± 5°C. The burner geometry limited optical excess to the flame root in the nozzle section, hence the flashback limits were evaluated based on the measurement of the nozzle surface temperature and visual observation of flame stability over the nozzle. To obtain independent evidence of surface roughness effects,
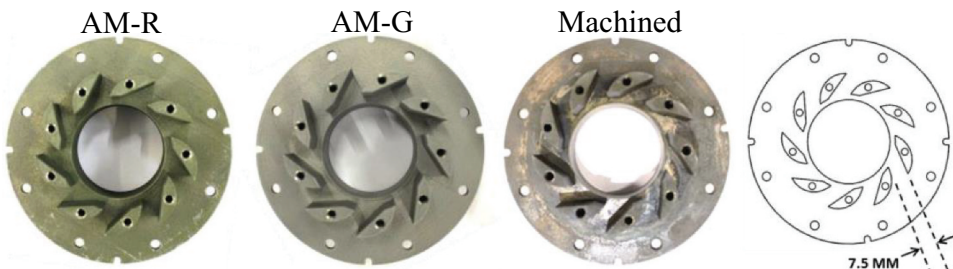

Figure 1. AM swirler vanes, $S_N = 0.8$; AM-R (A), AM-G (B), machined (C) (Runyon et al. 2019).

the study employed integrated diagnostic tools, including continuous gaseous emission sampling (NO_x and O_2), systematic measurements of single-point gas temperatures and high-speed OH* chemiluminescence. Flame shape and location were visualized through high-speed imaging of the OH* radical. Excess O_2 measurements were utilized to confirm the equivalence ratio for the three swirlers. Further details of the diagnostic tools and measuring equipment are presented in Section 3.2. The repeatability of the test points for each swirler was evaluated and reported within.

Experimental set-up

Atmospheric pressure generic swirl burner (APGSB)

The Atmospheric Pressure Generic Swirl Burner (APGSB) utilized in this study, depicted in Figure 2, is a direct geometrical replica of the High-Pressure Generic Swirl Burner (HPGSB) Mk. II, which has been extensively characterized previously (e.g., Pugh et al. 2018; Runyon 2017; Runyon et al. 2015, 2017), enabling comparison of results. Schematics of the cross-section and side view of the HPGSB Mk.II and APGSB are presented in Figure 2(a,b), respectively. Further details regarding the burner design, dimensions, and features can be found elsewhere (Runyon 2017). The flame was contained within a quartz tube flame holder of 100 mm ID with a length of approximately 407 mm. A top hat was constructed of a custom Nimonic 80a alloy structure and placed at the exit of the quartz confinement, serving as a support structure for the emissions probe of the gas analyzer. The air and fuel delivery to the APGSB was achieved through a dedicated supply system, allowing the
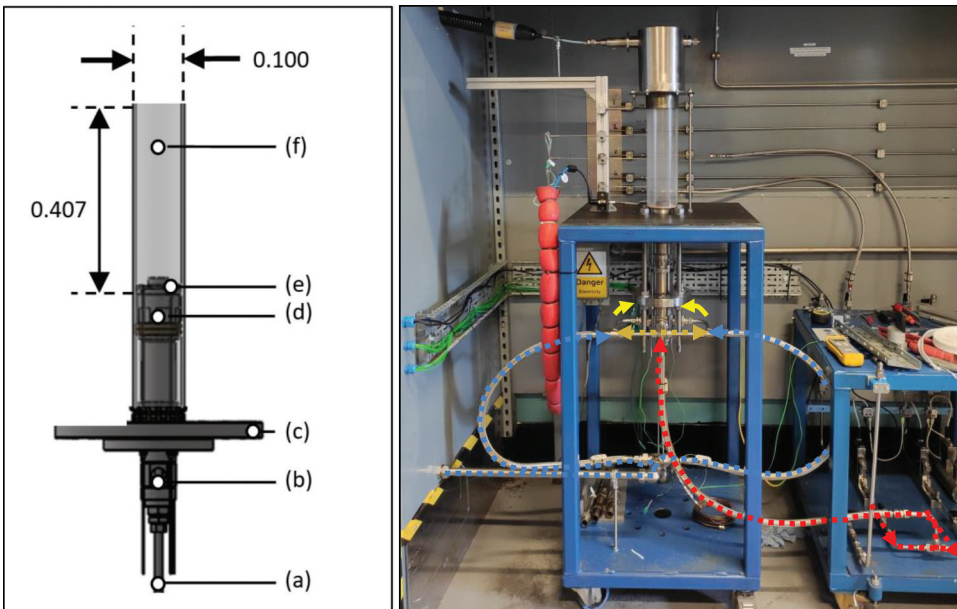

Figure 2. (a) schematic of HPGSB Mk.II showing instrumentation and pilot lance (a), inlet plenum (b), HPOC connecting flange (c), mixing chamber (d), burner exit nozzle (e), and quartz confinement (f). Dimensions in meters. Source (Runyon 2017).: (B) Assembled APGSB test rig during commissioning stage, indicating air (blue dotted line), fuel (red dotted line) and mixture (yellow arrows) delivery paths.

delivery of air and fuel at controlled temperatures and flow rates. For the fuel supply, Bronkhorst miniCORI-FLOW M14V11l mass flow controllers were used, capable of supplying flows up to 8 g/s, with an uncertainty of ± 0.5% of full-scale. Regarding air delivery, an IN-FLOW F-203Al industrial-style thermal mass flow controller was utilized, capable of delivering up to 25 g/s, with an uncertainty of ± 0.5% of full-scale. For the specialized cases where more air flow rate was required, two mass flow controllers were used in parallel. The path of inlet air and fuel is presented in Figure 2(b).

High-speed OH* chemiluminescence system

The high-speed OH* chemiluminescence system used in the study is shown in Figure 3(a). The system comprises a high-speed camera relay lens and image intensifier, UV lens (Ricoh FL-GC7838-VGUV, f/16), and 310 nm narrow bandpass filter. The high-speed camera is a monochromatic Vision Research Phantom v1212 (12-bit 12,000 frames/second at full 1280×800 resolution) controlled using Vision Research PCC 2.8 and Specialised Imaging Limited SILControl2 software. For each test point, 2000 images were acquired at the frame rate of 4000 Hz, corresponding to a recording time of 0.5 s, with an intensifier gate time of 10 μs utilized at constant gain. The resultant field of view was approximately 157 mm by 162 mm in the radial (x) and axial (y) direction at the camera resolution of 544×648 pixels, providing a resolution of approximately 3.46 pixels/mm. Several imaging techniques were subsequently used to post-process the recorded images before the reconstruction of Abel-deconvoluted OH* chemiluminescence images, involving noise filtering through a 3×3 pixel median filter, background intensity subtraction, and temporal averaging. An open-source MATLAB code developed by Killer (Killer 2016) based on the Abel transformation method reported by Pretzel (Pretzel 1991) was applied to identify the flame structure.
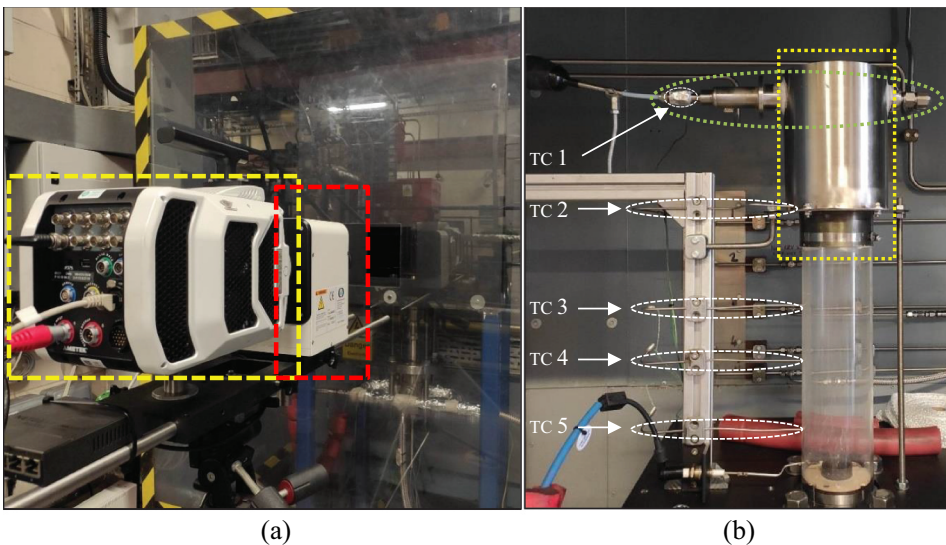

Figure 3. (a) Experimental set-up view with the high-speed camera (Yellow rectangular section) and intensifier (red rectangular section) aligned in front of the APGSB burner. (b) Combustion and exhaust section of APGSB, indicating the metallic sampling probe support structure (yellow dotted rectangular section), the water-cooled probe (green dotted oval section) and the various K-type thermocouples (TCs).

Exhaust gas analysis

An industry standard exhaust gas emission system, provided by Signal Gas Analysers Ltd., was operated for sampling the exhaust gases. The sample handling system comprises a multi-point equal area probe connected to a water-cooled tube in tube heat exchanger used to condition the sample to 160°C, before subsequent transfer, using a heated diaphragm pump, through heated lines and filter units to a distribution oven that delivered hot wet sample gas to the NO_x CLD and to a chiller prior to the dry O_2 paramagnetic sensor. The temperature was maintained constant at 160°C throughout the sample handling system. NO_x concentrations were quantified by a heated vacuum chemiluminescence analyzer (Signal Instruments 4000VM). O_2 concentrations were detected in the dry sample using a paramagnetic analyzer (Signal 9000MGA). All NO_x concentrations captured were normalized to equivalent dry conditions ($NO_{x,\ dry}$), according to Eqn. (9) ISO-11,042 (British Standard ISO 11,042–1:1996), before being further normalized to equivalent 15% O_2 according to Eqn. (10) ISO-11,042 (British Standard ISO 11,042–1:1996). Concerning the uncertainty of the measurement, it was calculated at approximately 2 ppmv, accounting for analyzer specifications, linearization, accuracy in span gas specifications and the drift in the measurements.

Thermocouples

To appraise the combustion performance of the three swirlers of different surface roughness, while monitoring the system and ensuring safe and reliable operation, several pre-calibrated K-type thermocouples were instrumented around the APGSB, as shown in Figure 3(b). Other than TC 1, which was an exposed junction thermocouple monitoring the water-cooled emissions probe, the thermocouples were 310 stainless steel sheathed K-type . These instruments were suitable for continuous exposure up to +1100°C, with a maximum temperature rating of ≈ 1350°C. Regarding the measurement uncertainty in temperature, it was estimated as ± 2.2°C as per the manufacturers' specifications. The data was collected and logged in real-time at 10 Hz over 60 s. Three thermocouples were placed on the quartz glass confinement (TC3, TC4, and TC5) for surface temperature monitoring, while another (TC2) was placed in the exhaust section of the burner, aligned with its centerline, to capture the transient behavior of the exhaust gas stream temperature. Across all the test points investigated, the maximum standard deviation of the exhaust gas temperature was circa 1%.

Results

Stability maps

The present study investigated the influence of surface roughness on LBO and FB limits for the two AM swirlers (AM-G & AM-R), in comparison to the traditionally manufactured "Machined" benchmark. Additionally, the study compared the operational stability of pure H_2 and CH_4/H_2 flames against pure CH_4 flames to explore differences resulting from the thermo-diffusive properties of hydrogen. For the CH_4 case, FB could not be achieved at 25 kW for the current burner configuration, as the bulk flow velocity of the mixture remained higher than the flame-speed, even at near-stoichiometric conditions, where the flame-speed is estimated to reach its maximum. A "technical
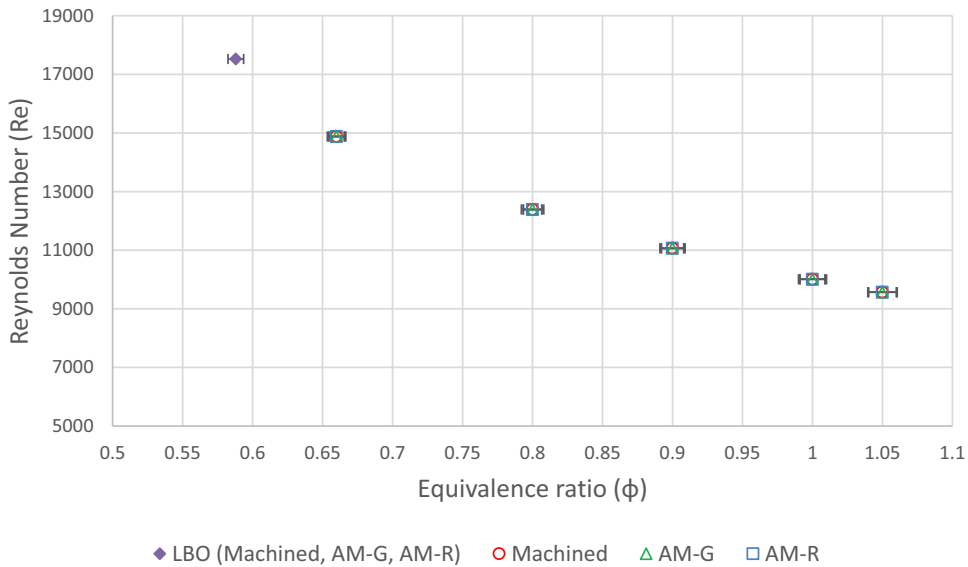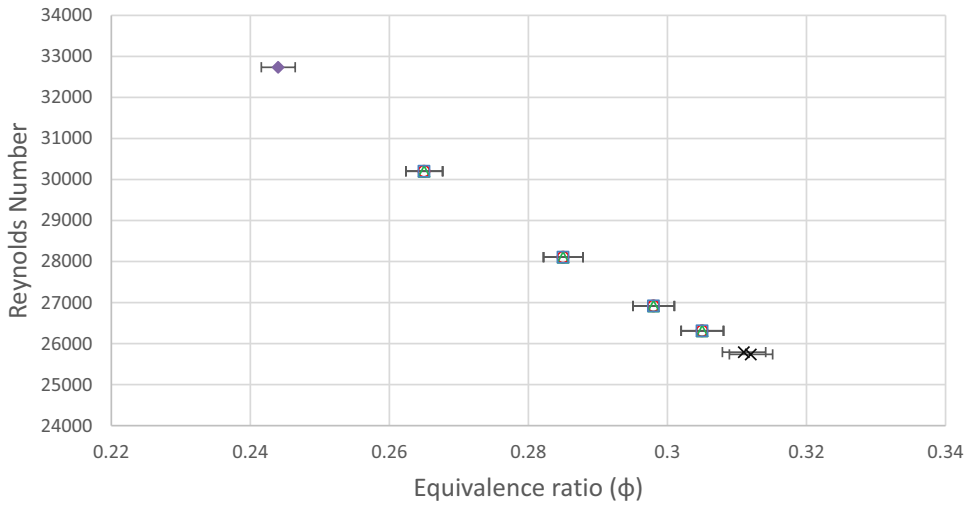
Figure 4. Stable operating trends for 100% CH$_4$ with machined, am-G and AM-R swirlers.

flashback point" (TFP) was, therefore, chosen as the upper limit of the stable operating curve ($\varphi = 1.05$). Figure 4 presents the burner stability envelopes of the three swirlers for 100% CH$_4$ flames as a function of Reynolds number and equivalence ratio. The horizontal error bars in the figure relate to the uncertainty of the mass flow rate, and hence equivalence ratio variations. It is observed that uncertainties remained sufficiently small, around 1% in the overall test points.

It is observed that within the relative uncertainty the three swirlers of different surface roughness demonstrated the same flame stability behavior, with almost identical TFP and LBO limits at $\varphi = 1.05 \pm 1\%$ and $\varphi = 0.558 \pm 1\%$, respectively. This trend indicates a negligible effect of surface roughness on the CH$_4$ flames under the test conditions investigated, in agreement with previous investigations (Runyon et al. 2019).

Figures 5 and 6 demonstrate the burner stability map for the 100% H$_2$ and 23%$_{vol}$CH$_4$/77%$_{vol}$H$_2$ fuel blends, respectively. In contrast to the 100% CH$_4$ flames, flashback events were observed for the 100% H$_2$ and 23%$_{vol}$CH$_4$/77%$_{vol}$H$_2$ flames. For the pure H$_2$ flames, the flashback points of the three swirlers overlapped at $\varphi = 0.311 \pm 1\%$ regardless of the surface roughness (see Figure 5). For the 23%$_{vol}$CH$_4$/77%$_{vol}$H$_2$ blend, the flashback propensity slightly shifted from $\varphi = 0.458 \pm 1\%$ (Machined) to $\varphi = 0.450 \pm 1\%$ (AM-R) with increasing surface roughness (see Figure 6), though it is noted this difference is within the stated uncertainty of the mass flow controller. The variation in the FB limit owing to surface roughness was expected to be small due to the small range of surface roughness (Runyon et al. 2019). The LBO limits for the pure H$_2$ case and the CH$_4$/H$_2$ blend were detected at $\varphi = 0.244 \pm 1\%$ and $\varphi = 0.327 \pm 1\%$, correspondingly. For both cases, surface roughness was found to have a minimal impact on LBO instability since for the three swirlers the LBO limits were identified under nominally similar equivalence ratios and were characterized by the same instability mechanism. This is likely due to the minor effect of the surface roughness height on modifying the bulk flow velocity against the flame speed.

Figure 5. Stable operating trends for 100% H$_2$ with machined, am-G and AM-R swirlers.
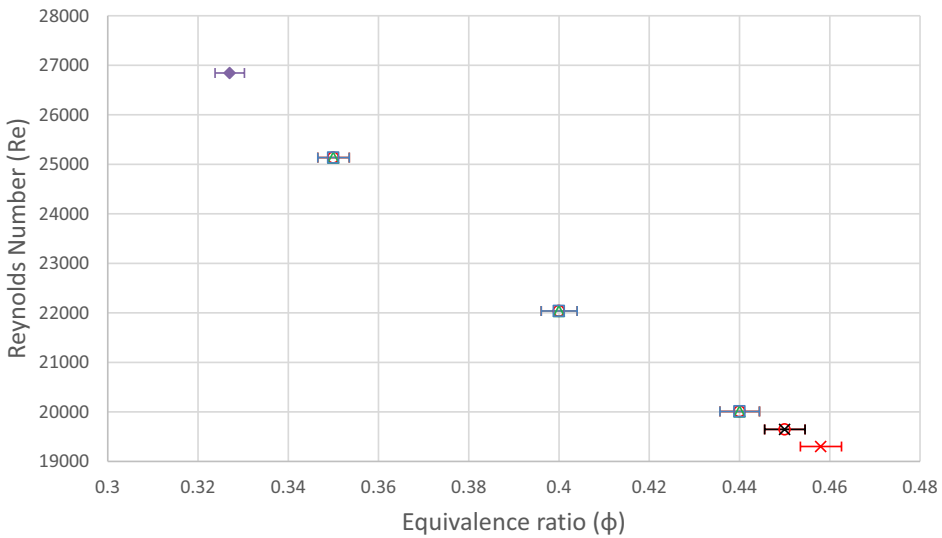
Figure 6. Stable operating trends for 23%$_{vol}$CH$_4$/77%$_{vol}$H$_2$ with machined, am-G and AM-R swirlers.

Regardless of the surface roughness, the H$_2$ content in the fuel mix has a significant effect on modifying the burner operability regime. Maintaining the same thermal power output, switching from 100% CH$_4$ through 23%$_{vol}$CH$_4$/77%$_{vol}$H$_2$ to 100% H$_2$ modifies the amount of air flow to be introduced into the system to balance the flame speed. Therefore, the stable operating curve spread across different equivalence ratios and Reynolds numbers based on fuel compositions. As seen in Figures 4–6, the burner stability envelope was shifted toward leaner equivalence ratios with increased H$_2$ percentage in the fuel mix due to the higher

reaction rate, burning velocity, and diffusivity associated with H_2 combustion. Consequently, the lean flammability limits were extended, and the LBO occurred at leaner conditions for the higher H_2 content of fuel mixes. This is consistent with several previous experimental studies (Kim, Arghode, and Gupta 2009; Liu et al. 2021; Schefer 2003; Tuncer, Acharya, and Uhm 2009; Kim et al. 2009). Specifically, the LBO limit was lowered by around 41% for $77\%_{vol}H_2$ ($\varphi = 0.327 \pm 1\%$) enrichment in CH_4 and almost 60% for 100% H_2 ($\varphi = 0.244 \pm 1\%$), compared to baseline 100% CH_4 ($\varphi = 0.558 \pm 1\%$). The enhanced flammability limits by H_2 addition could be related to the thermo-diffusive properties of H_2 under lean turbulent conditions, in which the flame stretch accelerates the flame, resulting in higher burning velocities (Lapalme, Lemaire, and Seers 2017), consequently improving the resistance of the flame to combustion instabilities (Fairweather et al. 2009; Lapalme, Lemaire, and Seers 2017).

An increased H_2 content in the fuel mix significantly narrowed the operability range of the burners. For the 100% CH_4 flames, the stable operating curves of the "Machined" swirler, ranged from $0.558 < \varphi < 1.05$ (Figure 4), whereas the stability limits of $23\%_{vol}CH_4/77\%_{vol}H_2$ and 100% H_2, were reduced to a narrower equivalence range $0.327 < \varphi < 0.458$ (Figure 5) and $0.244 < \varphi < 0.312$ (Figure 6), respectively. This is qualitatively consistent with previous experimental studies utilizing a range of H_2 fuel blends (Runyon 2017; Syred et al. 2012). The narrow operability limits of H_2-enriched flames impose significant technical challenges in burning hydrogen fuels in large-scale power plants, as even minor variations in operating conditions (inlet temperature, air/fuel mixture concentration, and pressure) could potentially result in blow-off or flashback phenomena, risking the power plant's operation and durability. This challenge was also issued in identifying the FB limits for the H_2 enriched flames, in which the flashback limits determined were within the quoted error bars.

NO_x emissions

Figure 7 presents the results of the investigation on the normalized NO_x emissions (dry, 15% O_2) for the three swirl burners for CH_4/air mixtures. The error bars in the figure
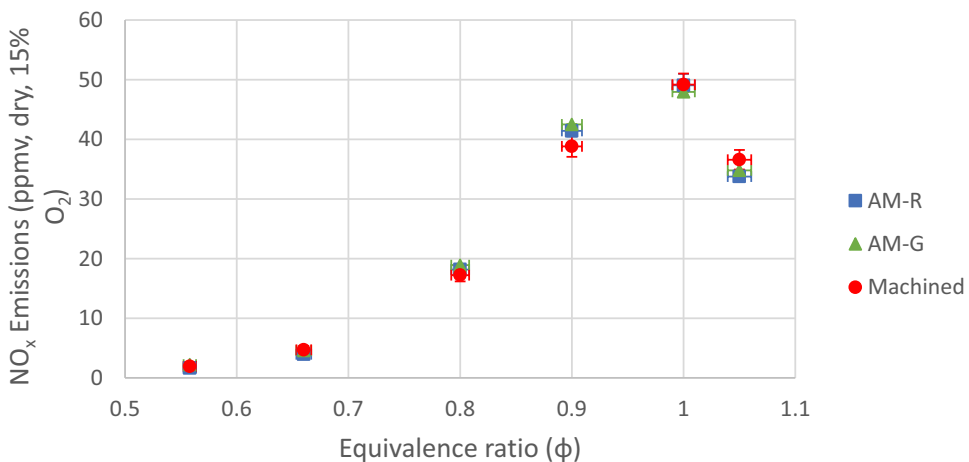

Figure 7. Average NO_x emissions indicating repeatability for CH_4/air mixtures.

represent the standard deviations of the repeated data sets. The data was dispersed around 5–10% of the average mean values (≈2–4 ppmv) for φ > 0.66, complying with the uncertainty requirement of the BS-EN standard 14,792:2017. The NO_x emissions showed substantial variations with the surface roughness toward the fuel-rich conditions, particularly at φ = 0.9 and φ = 1.1, in which the AM-R and AM-G exhibited an observable difference from the "Machined" swirler, though being within the standard measuring error of the experiments.

Figures 8 and 9 show the variation of the normalized NO_X emissions (dry, 15% O_2) across the equivalence ratio for the pure H_2 and 77%$_{vol}$$H_2$/23%$_{vol}$$CH_4$ flames, respectively. However, the analysis did not give any solid evidence to draw a statistically significant conclusion regarding the surface roughness effect, as it is noted the error bars overlap with differences in measured NO_X emissions of less than 2 ppmv. However, the lean premixed
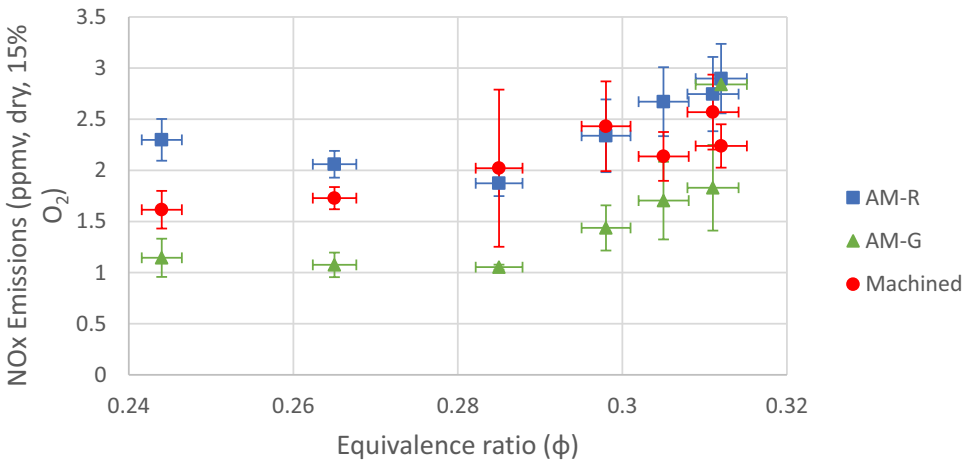

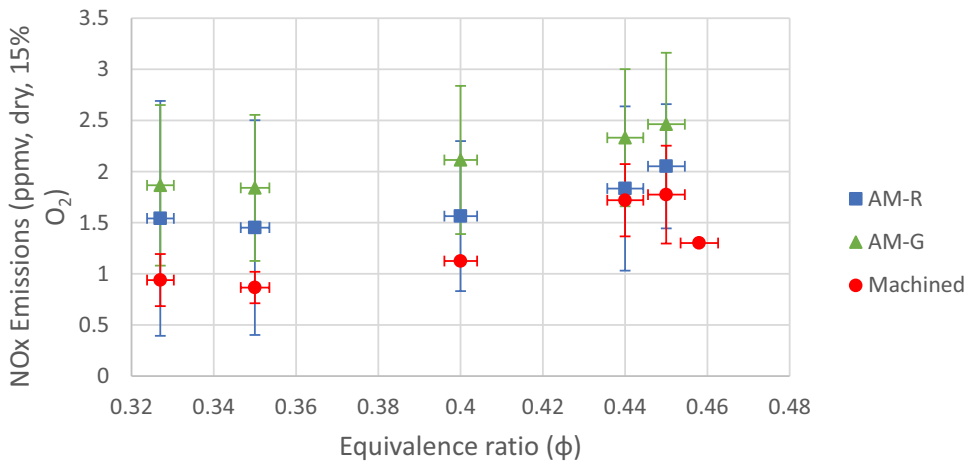**Figure 8.** Average NO_x emissions indicating repeatability for H_2/air mixtures.

Figure 9. Average NO_x emissions indicating repeatability for CH_4/H_2 fuel mixtures.

H_2 flames under the considered test conditions showed significantly lower NO_x emissions across their flammability limits when compared with the pure CH_4 flames. This is due to the suppression of the thermal NO_x contribution to the total NO_x formation due to the lower relative reactivity of hydrogen flames at very lean conditions. These observations are consistent with previous experimental studies investigating the effect of H_2 enrichment in CH_4 with respect to NO_x emissions (Griebel, Boschek, and Jansohn 2007; Tuncer, Acharya, and Uhm 2009).

Exhaust temperatures

Figures 10–12 present the gas temperature variations across equivalence ratios for the three different fuel blends and swirlers. In contrast to the NO_x emissions, the three swirlers of the
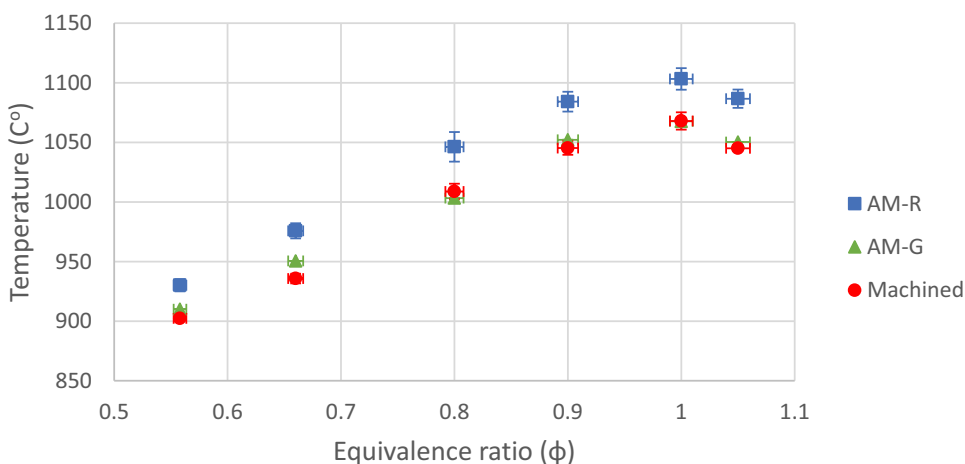

Figure 10. Average exhaust thermocouple temperature indicating repeatability for CH_4/air mixtures.
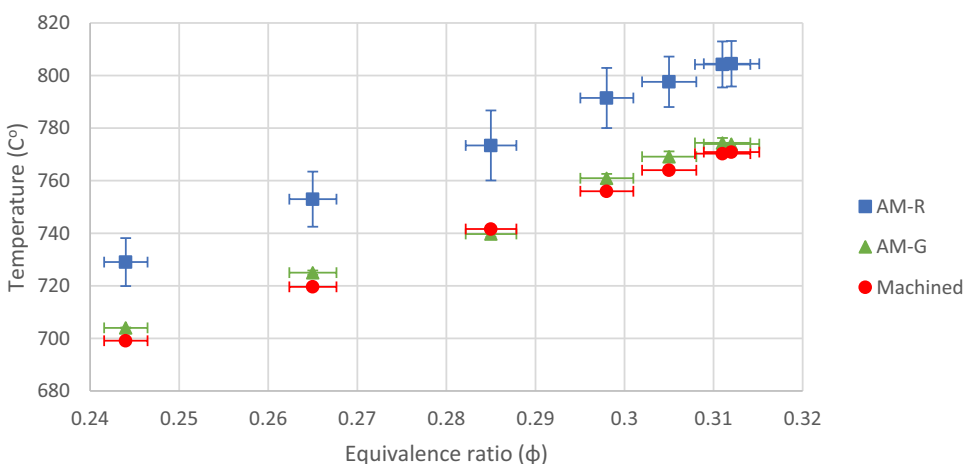

Figure 11. Average exhaust thermocouple temperature indicating repeatability for H_2/air mixtures.
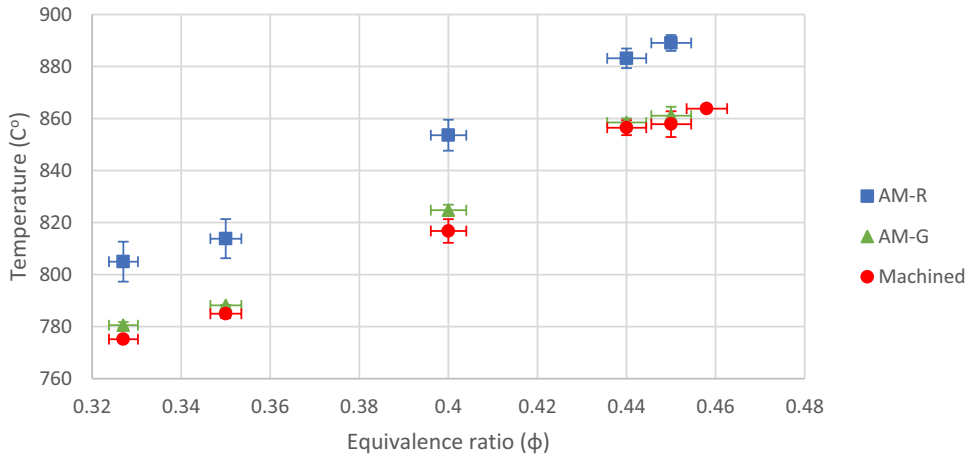
Figure 12. Average exhaust thermocouple temperature indicating repeatability for CH_4/H_2 mixtures.

different surface roughness (1–9 µm) yielded statistically validated differences in the exhaust temperatures at the center of the exit plane. The AM-R swirler was found to systematically produce higher exhaust temperatures, followed by the AM-G and "Machined" swirler, which showed similar readings. The difference in exhaust temperature between the AM-R and the "Machined" swirlers was approximately $\approx 40°C$ for the pure CH_4 case, which reduced to $\approx 29°C$ and $\approx 25°C$ for the blend and pure H_2 cases, respectively. The analogous difference between the "Machined" and the AM-G swirlers was substantially lower and equal to $\approx 5°C$ for most equivalence ratios across the range of fuels. Compared to the 100% CH_4 case, the resultant exhaust temperatures were also significantly lower for the two alternative fuel cases. This is consistent with the lower NO_x emissions recorded under pure H_2 and CH_4/H_2 combustion.

Since all profiles were measured using the same pre-calibrated K-type thermocouple mounted at the same location, the differences in exhaust temperature should not stem from inconsistencies of the measurement setup. Moreover, since the inlet plenum temperature was within the acceptable level of deviation of $150 \pm 5°C$, these differences are not likely owing to the physical properties of the mixture. This was further confirmed by the NO_x emissions, which were within similar levels, which confirmed approximately equal flame temperatures. Therefore, it is proposed that the observed temperature differences in the exhaust stem from variations in the flow field aerodynamics and subsequently, the stabilization location of the flame resultant from changes in surface roughness. To investigate the validity of this hypothesis, further experimental investigations were undertaken utilizing high-speed OH* chemiluminescence measurements of the flame, to confirm the flame location under stable operation.

Flame locations

Figure 13 shows examples of Abel deconvoluted OH* chemiluminescence images for 100% CH_4 ($\varphi = 0.80$), $77\%_{vol}H_2/23\%_{vol}CH_4$ ($\varphi = 0.40$), and 100% H_2 ($\varphi = 0.285$) flames, including the weighted centroid of the flame area as represented by a black "dot" on each image. The
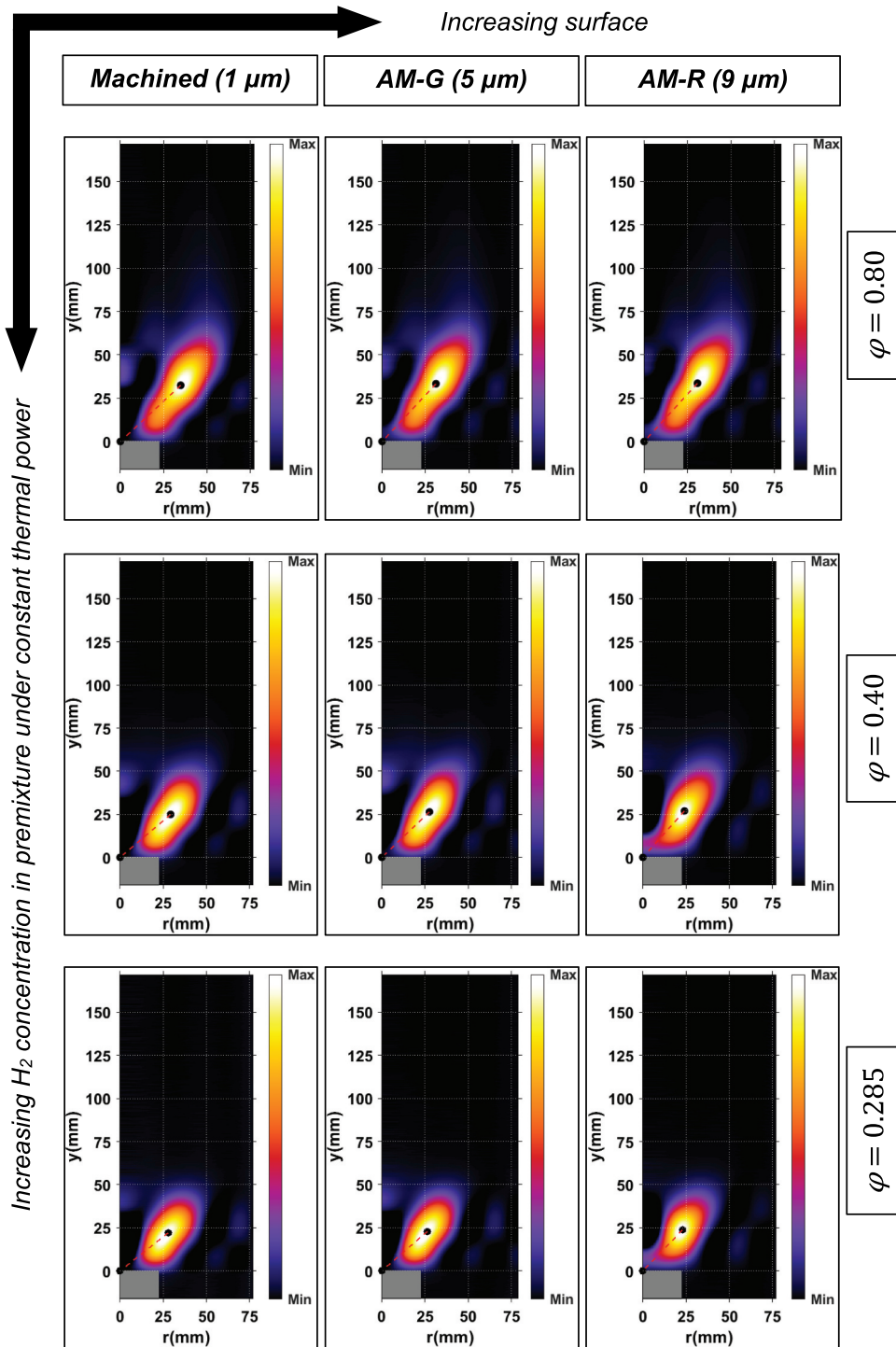
Figure 13. Deconvoluted OH* chemiluminescence results for the three swirlers at φ = 0.80 (CH$_4$), φ = 0.40 (CH$_4$/H$_2$) and φ = 0.285 (H$_2$).

weighted centroid was constructed on the Abel deconvoluted images through the standard MATLAB operators. Regardless of the fuel type, the weighted centroid of the flame area slightly moved toward the centerline of the burner ($r = 0$) with increasing surface roughness. Apart from the visual observations, the shifting was quantified in the cartesian plane, across all equivalence ratios, shown in Figures 14–16, for 100% CH_4, $77\%_{vol}H_2/23\%_{vol}CH_4$ and 100% H_2, respectively.

For all the fuel types tested, noticeable changes in the x-coordinate of the flame centroid were noted for the swirlers of different surface roughness, with the stable flame location appearing closer to the centerline of the burner for relatively rougher surfaces, which is in qualitative agreement with other studies (Runyon et al. 2019). For the 100% CH_4 and the $77\%_{vol}H_2/23\%_{vol}H_2$ cases, this difference of the x-coordinate of the flame centroid between
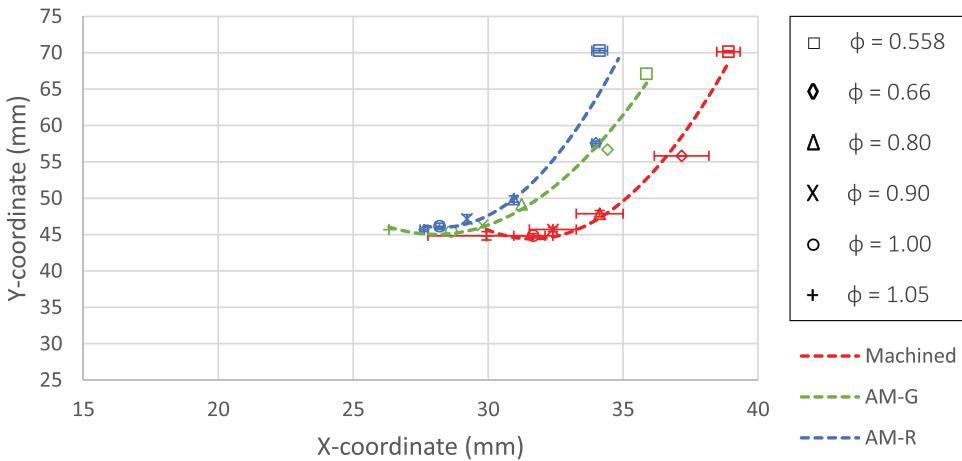

Figure 14. Flame centroids cartesian coordinates across the equivalence ratio range for CH_4/air mixtures with machined (1 μm), AM-G (5 μm) and AM-R (9 μm) swirlers.
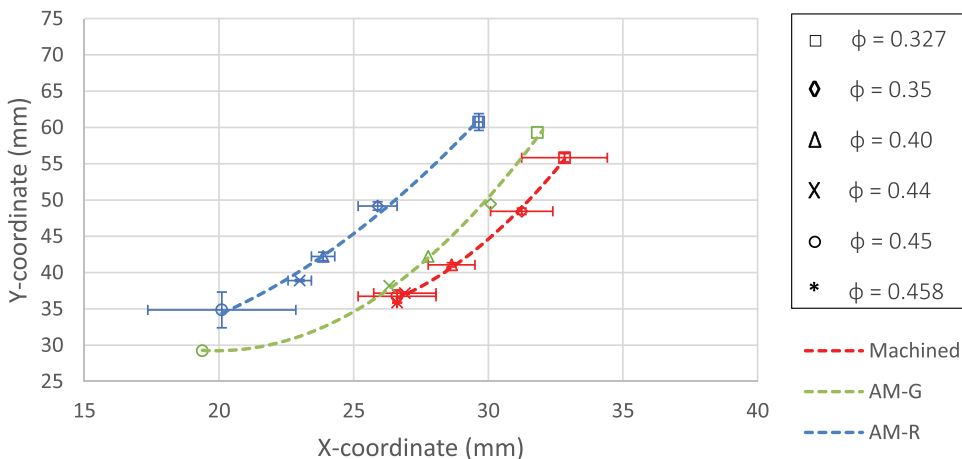

Figure 15. Flame centroids cartesian coordinates across the equivalence ratio range for CH_4/H_2 fuel mixtures with the machined (1 μm), AM-G (5 μm) and AM-R (9 μm) swirlers.
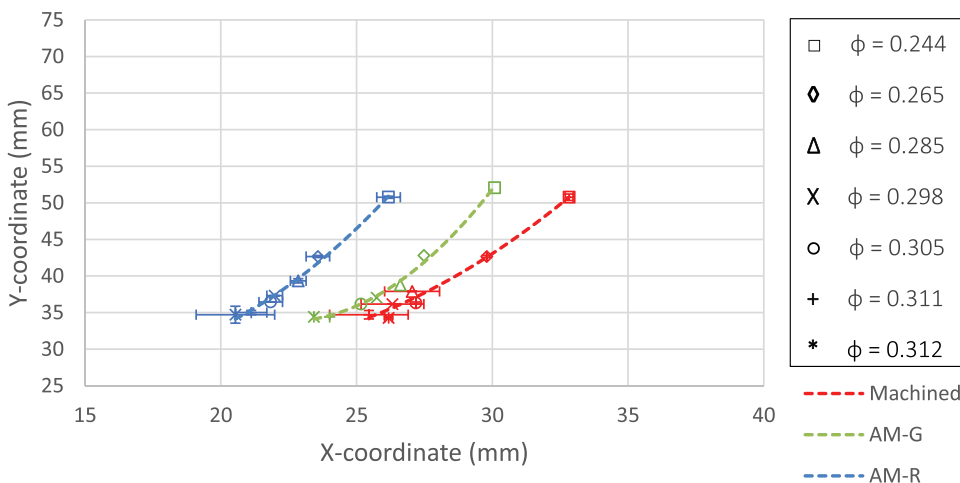
Figure 16. Flame centroids cartesian coordinates across the equivalence ratio range for H₂/air mixtures with the machined (1 μm), AM-G (5 μm) and AM-R (9 μm) swirlers.

the "Machined" and the AM-R swirlers was equal to ≈4 mm, whilst for the 100% H₂ case, the analogous change was ≈6 mm. The most considerable difference between the "Machined" and the AM-R swirler was found for each fuel tested at its corresponding LBO limit. This marginal difference can be explained by the fact that the Reynolds number was at its maximum, and so the surface roughness for this case was expected to have a more significant impact due to the increased surface roughness/boundary layer thickness ratio (Kadivar, Tormey, and McGranaghan 2021). As discussed, for the increased surface roughness cases, the flame stabilized closer to the centerline of the burner corresponding with the aforementioned higher temperatures recorded by the exhaust thermocouple, which was located on the centerline. It is noted that the increase in temperature corresponded only to a single point and should not be confused with a spatially averaged temperature value across the diameter of the exhaust, which would explain the resultant similar NO_x emissions measured.

Regardless of the surface roughness and the fuel type, along the stability curve (LBO to FB), the y-coordinate of the flame centroids decreases. This decrease was ≈25 mm for the pure CH_4 and the CH_4/H_2 blend cases, and ≈15 mm for the pure H_2 case where the flame had already more compact shape due to the thermodynamic properties of hydrogen and equivalence ratio variation. This behavior can be explained by the modification of bulk flow velocity and, thus, flame location with the equivalence ratio. When airflow decreases at a constant fuel flow, the equivalence ratio increases toward the stoichiometry, which in turn decreases bulk flow velocity and increases the flame speed (Law 2006). This change in the flame speed with respect to bulk flow velocity causes the flame location to shift. As a result, the flame retreats closer to the nozzle exit.

Conclusions

Additive Manufacturing not only enables the control of the resultant surface roughness during the fabrication stage of the component but also potentially minimizes the need for

post-processing, leading into potential cost and lead-time reductions. In this context, empirical and image processing methods were developed and applied to evaluate the influence of surface roughness on burner characteristics and combustion performance for CH_4, CH_4/H_2 blended and H_2 fuels. Image processing enabled the flame centroids to be located, which were found to shift closer to the centerline of the burner as the swirlers' surface roughness increases. Variation of surface roughness also altered the aerodynamic flow field in a such way that the flame was stabilized and aligned closer to the burner axis, where highest temperature readings were recorded for the AM-R swirler. Despite the altered flame location, the surface roughness heights selected did not significantly influence the burner stability envelopes and NO_x emissions performance of the swirl burner, the latter considered due to temperature spatial-averaging across the exhaust. For all fuel types tested, the swirlers manufactured using additive layer (AM-R and AM-G) resulted in combustion performance comparable to the traditionally manufactured Machined swirler, indicating from a practical perspective for manufacturers of additive layer parts, that there are negligible performance advantages in post-manufacture surface finishing, which could be an important consideration concerning production cost reductions.

Acknowledgements

Disclosure statement

No potential conflict of interest was reported by the author(s).

Funding

References

Al-Fahham, M., S. Bigot, and A. Valera Medina. 2016. A study of fluid flow characteristics using micro structured surfaces produced by WEDM. *4M/IWMF2016 The Global Conference on Micro Manufacture*, 247–50. doi:10.3850/978-981-11-0749-8_708.

Al-Fahham, M., F. A. Hatem, Z. Al-Dulami, A. V. Medina, and S. Bigot. 2017. Experimental study to enhance swirl burner against boundary layer flashback. *Energy Procedia* 142:1534–38. doi:10.1016/j.egypro.2017.12.604.

An, Q., S. Kheirkhah, J. Bergthorson, S. Yun, J. Hwang, W. J. Lee, M. K. Kim, J. H. Cho, H. S. Kim, and P. Vena. 2021. Flame stabilization mechanisms and shape transitions in a 3D printed, hydrogen enriched, methane/Air low-swirl burner. *Int. J. Hydrogen Energy* 46 (27):14764–79. doi:10.1016/j.ijhydene.2021.01.112.

Berger, L., A. Attili, and H. Pitsch. 2022. Synergistic interactions of thermodiffusive instabilities and turbulence in lean hydrogen flames. *Combust. Flame* 244:112254. doi:10.1016/j.combustflame.2022.112254.

Bons, J. P. 2010. A review of surface roughness effects in gas turbines. *J. Turbomach.* 132 (2):1–16. doi:10.1115/1.3066315.

Bons, J. P., S. T. McClain, Z. J. Wang, X. Chi, and T. I. Shih. 2008. A comparison of approximate versus exact geometrical representations of roughness for CFD calculations of Cf and St. *J. Turbomach.* 130 (2). doi: 10.1115/1.2752190.

Crayford, A. P., F. Lacan, J. Runyon, P. J. Bowen, S. Balwadkar, J. Harper, and D. G. Pugh. 2019. Manufacture, characterization and stability limits of an AM prefilming air-blast atomizer. *Proc. ASME Turbo. Expo.* 4B (2019):1–9. doi:10.1115/GT2019-91624.

Darcy, H. 1857. *Recherches Experimentales Relatives Au Mouvement de l'eau Dans Les Tuyaux [Experimental research relating to the movement of water in pipes]*. Paris: Mallet-Bachelier.

Dean, B., and B. Bhushan. 2010. Shark-skin surfaces for fluid-drag reduction in turbulent flow: A review. *Phil. Trans. R. Soc. A.* 368 (1929):4775–806. doi:10.1098/rsta.2010.0201.

Domel, A. G., M. Saadat, J. C. Weaver, H. Haj-Hariri, K. Bertoldi, and G. V. Lauder. 2018. Shark skin-inspired designs that improve aerodynamic performance. *J. R. Soc. Interface.* 15 (139):20170828. doi:10.1098/rsif.2017.0828.

ETN Global. 2020. Hydrogen gas turbines, 28. Accessed July 20, 2024. https://etn.global/wp-content/uploads/2020/01/ETN-Hydrogen-Gas-Turbines-report.pdf.

Fairweather, M., M. P. Ormsby, C. G. W. Sheppard, and R. Woolley. 2009. Turbulent burning rates of methane and methane-hydrogen mixtures. *Combust. Flame* 156 (4):780–90. doi:10.1016/j.combustflame.2009.02.001.

Fan, Y., T. Tsujimura, N. Iki, O. Kurata, and H. Furutani. 2021. Investigation of non-premixed hydrogen-oxygen impinged jet flame under steam dilution. *Proc. ASME Turbo. Expo.* 3B (2021):1–6. doi:10.1115/GT2021-59425.

Fanning, J. T. 1886. *A practical treatise on hydraulic and water-supply engineering*. New York, USA: D. Van Nostrand Company.

Goldmeer, J. 2019. *Power to gas: Hydrogen for power generation*. USA: General Electric Company.

Griebel, P., E. Boschek, and P. Jansohn. 2007. Lean blowout limits and NOx emissions of turbulent, lean premixed, hydrogen-enriched methane/air flames at high pressure. *J. Eng. Gas Turbines Power* 129 (2):404–10. doi:10.1115/1.2436568.

Hatem, F. A., A. S. Alsaegh, M. Al-Faham, and A. Valera-Medina. 2017. Enhancement flame flashback resistance against CIVB and BLF in swirl burners. *Energy Procedia* 142:1071–76. doi:10.1016/j.egypro.2017.12.358.

Jayakumar, A., D. K. Madheswaran, A. M. Kannan, U. Sureshvaran, and J. Sathish. 2022. Can hydrogen be the sustainable fuel for mobility in India in the global context? *Int. J. Hydrogen Energy* 47 (79):33571–96. doi:10.1016/j.ijhydene.2022.07.272.

Kadivar, M., D. Tormey, and G. McGranaghan. 2021. A review on turbulent flow over rough surfaces: Fundamentals and theories. *Int. J. Thermofluids* 10:100077. doi:10.1016/j.ijft.2021.100077.

Killer, C. 2016. Abel inversion algorithm. Matlab. Accessed July 20, 2024. https://www.mathworks.com/matlabcentral/fileexchange/43639-abel-inversion-algorithm.

Kim, H. S., V. K. Arghode, and A. K. Gupta. 2009. Flame characteristics of hydrogen-enriched methane-air premixed swirling flames. *Int. J. Hydrogen Energy* 34 (2):1063–73. doi:10.1016/j.ijhydene.2008.10.035.

Kim, H. S., V. K. Arghode, M. B. Linck, and A. K. Gupta. 2009. Hydrogen addition effects in a confined swirl-stabilized methane-air flame. *Int. J. Hydrogen Energy* 34 (2):1054–62. doi:10.1016/j.ijhydene.2008.10.034.

Lapalme, D., R. Lemaire, and P. Seers. 2017. Assessment of the method for calculating the Lewis number of H2/CO/CH4 mixtures and comparison with experimental results. *Int. J. Hydrogen Energy* 42 (12):8314–28. doi:10.1016/j.ijhydene.2017.01.099.

Larfeldt, J., M. Andersson, A. Larsson, and D. Moëll. 2017. Hydrogen Co-firing in siemens low NOx industrial gas turbines, POWER-GEN Europe, Cologne, Germany, 27–29.

Law, C. K. 2006. *Combustion physics*. New Jersey, USA: Cambridge University Press.

Li, P., D. Guo, and X. Huang. 2020. Heat transfer enhancement, entropy generation and temperature uniformity analyses of shark-skin bionic modified microchannel heat sink. *Int. J. Heat Mass Transf.* 146:118846. doi:10.1016/j.ijheatmasstransfer.2019.118846.

Liu, W., H. Ni, P. Wang, and Y. Zhou. 2020. An investigation on the drag reduction performance of bioinspired pipeline surfaces with transverse microgrooves. *Beilstein J. Nanotechnol.* 11:24–40. doi:10.3762/bjnano.11.3.

Liu, X., M. Bertsch, A. A. Subash, S. Yu, R. Z. Szasz, Z. Li, P. Petersson, X. S. Bai, M. Aldén, and D. Lörstad. 2021. Investigation of turbulent premixed methane/air and hydrogen-enriched methane/air flames in a laboratory-scale gas turbine model combustor. *Int. J. Hydrogen Energy* 46 (24):13377–88. doi:10.1016/j.ijhydene.2021.01.087.

Liu, X., X. Han, G. Yin, X. Song, and L. Cui. 2023. Design and processing of gas turbine blades based on additive manufacturing technology. *Micromachines* 14 (9):1675. doi:10.3390/mi14091675.

Lu, D., Z. Liu, X. Wei, C. Chen, and D. Wang. 2023. Effect of post-processing methods on the surface quality of Ti6Al4V fabricated by laser powder bed fusion. *Front. Mater.* 10. doi:10.3389/fmats.2023.1126749.

Moody, F. L. 1944. Friction factor for pipe flow. *Trans. A.S.M.E* 66 (8):671–78. doi:10.1115/1.4018140.

Mumtaz, K. A., and N. Hopkinson. 2010. Selective laser melting of thin wall parts using pulse shaping. *J. Mater. Process. Technol.* 210 (2):279–87. doi:10.1016/j.jmatprotec.2009.09.011.

National Academies of Sciences, Engineering, and Medicine. 2020. *Advanced technologies for gas turbines.* Washington, DC: The National Academies Press. doi:10.17226/25630.

Ngo, T. D., A. Kashani, G. Imbalzano, K. T. Q. Nguyen, and D. Hui. 2018. Additive manufacturing (3D printing): A review of materials, methods, applications and challenges. *Compos. Part B Eng.* 143:172–96. doi:10.1016/j.compositesb.2018.02.012.

Nikuradse, J. 1950. Laws of flow in rough pipes. *J. Appl. Phys.* 3:399.

Patel, S. 2018. 3-D printed gas turbine technology marks "game changing" milestone. *POWER Magazine*. Accessed July 24, 2024. https://www.powermag.com/3-d-printed-gas-turbine-technology-marks-game-changing-milestone/.

Prandi, R. 2019. One more GE's GT26 HE upgrade. *Diesel & gas turbine worldwide*. https://www.dieselgasturbine.com/news/One-More-GE-s-GT26-HE-Upgrade/7009340.article.

Pretzel, G. 1991. A new method for numerical abel-inversion. *Z. Für Naturforschung A.* 46 (7):639–41. doi:10.1515/zna-1991-0715.

Pugh, D., P. Bowen, A. Crayford, R. Marsh, J. Runyon, S. Morris, and A. Giles. 2018. Catalytic influence of water vapor on lean blow-off and NOx reduction for pressurized swirling syngas flames. *J. Eng. Gas Turbines Power* 140 (6):1–10. doi:10.1115/1.4038417 .

Runyon, J. 2017. *Gas turbine fuel flexibility: Pressurized swirl flame stability, thermoacoustics, and emissions.* Cardiff, Wales, UK: Cardiff University.

Runyon, J., A. Giles, R. Marsh, D. Pugh, B. Goktepe, S. Morris, D. Pugh, P. Bowen, and M. Steven. 2019. Characterization of ALM swirl burner surface roughness and its effects on flame stability using high-speed diagnostics. *Proc. ASME Turbo. Expo.* 4A:1–13. doi:10.1115/GT2019-90215.

Runyon, J., R. Marsh, D. Pugh, P. Bowen, A. Giles, S. Morris, and A. Valera-Medina. 2017. Experimental analysis of confinement and swirl effects on premixed Ch4-H2 flame behavior in a pressurized generic swirl burner. *Proc. ASME Turbo Expo. Part* F1300:1–12. doi:10.1115/GT2017-64794.

Runyon, J., R. Marsh, Y. Sevcenco, D. Pugh, and S. Morris. 2015. Development and commissioning of a chemiluminescence imaging system for an optically-accessible high-pressure generic swirl burner. *7th European Combustion Meeting*, Budapest, Hungary, 1–6, September.

Runyon, J., I. Psomoglou, R. Kahraman, and A. Jones. 2021. Additive manufacture and the gas turbine combustor: Challenges and opportunities to enable low-carbon fuel flexibility. *Gas Turbines in a Carbon-Neutral Society 10th International Gas Turbine Conference*, 1–17, October.

Schefer, R. W. 2003. Hydrogen enrichment for improved lean flame stability. *Int. J. Hydrogen Energy* 28 (10):1131–41. doi:10.1016/S0360-3199(02)00199-4.

Schlichting, H., and K. Gersten. 2014. Boundary layer theory. In *Aircraft engineering and aerospace technology*, vol. 7, 9th ed. doi:10.1108/eb029898.

Sinha, A., B. Swain, A. Behera, P. Mallick, S. K. Samal, H. M. Vishwanatha, and A. Behera. 2022. A review on the processing of aero-turbine blade using 3D print techniques. *J. Manuf. Mater. Process.* 6 (1):16. doi:10.3390/jmmp6010016.

Syred, N., M. Abdulsada, A. Griffiths, T. O'Doherty, and P. Bowen. 2012. The effect of hydrogen containing fuel blends upon flashback in swirl burners. *Appl. Energy* 89 (1):106–10. doi:10.1016/j.apenergy.2011.01.057.

Tuncer, O., S. Acharya, and J. H. Uhm. 2009. Dynamics, NOx and flashback characteristics of confined premixed hydrogen-enriched methane flames. *Int. J. Hydrogen Energy* 34 (1):496–506. doi:10.1016/j.ijhydene.2008.09.075.

UK Research and Innovation. 2020. Storage of ammonia for energy (SAFE) - AGT pilot. Accessed July 18, 2024. https://gtr.ukri.org/projects?ref=EP%2FT009314%2F1.

Velu, R., T. Calais, A. Jayakumar, and F. Raspall. 2020. A comprehensive review on bio-nanomaterials for medical implants and feasibility studies on fabrication of such implants by additive manufacturing technique. *Materials* 13 (1):92. doi:10.3390/ma13010092.

Walton, R. 2021. GE GT26 HE upgrade completed at Uniper UK plant, coming to Singapore, Buenos Aires. *Power Eng.* https://www.power-eng.com/om/plant-optimization/new-ge-gt26-he-upgrade-shows-benefits-in-uniper-uk-plant-testing/.

York, W., M. Hughes, J. Berry, T. Russell, Y. C. Lau, S. Liu, M. Arnett, A. Peck, J. Tralshawala, N. Weber, et al. 2015. *Advanced IGCC/Hydrogen gas turbine development*. Oek Reidge, TN. https://www.osti.gov/biblio/1261809.